

Observation of $e^+e^- \rightarrow \gamma\chi_{c1}$ and search for $e^+e^- \rightarrow \gamma\chi_{c0}, \gamma\chi_{c2}$, and $\gamma\eta_c$ at \sqrt{s} near 10.6 GeV at Belle

S. Jia,² X. L. Wang,⁹ C. P. Shen,² C. Z. Yuan,²⁵ I. Adachi,^{16,12} H. Aihara,⁸⁶ S. Al Said,^{80,34} D. M. Asner,³ H. Atmacan,⁷⁶ V. Aulchenko,^{4,64} T. Aushev,⁵³ R. Ayad,⁸⁰ V. Babu,⁸¹ V. Bansal,⁶⁶ P. Behera,²³ C. Beleño,¹¹ M. Berger,⁷⁷ B. Bhuyan,²¹ T. Bilka,⁵ J. Biswal,³¹ A. Bobrov,^{4,64} A. Bozek,⁶¹ M. Bračko,^{47,31} T. E. Browder,¹⁵ L. Cao,³² D. Červenkov,⁵ P. Chang,⁶⁰ V. Chekelian,⁴⁸ A. Chen,⁵⁸ B. G. Cheon,¹⁴ K. Chilikin,⁴¹ K. Cho,³⁶ S.-K. Choi,¹³ Y. Choi,⁷⁸ S. Choudhury,²² D. Cinabro,⁹⁰ S. Cunliffe,⁷ N. Dash,²⁰ S. Di Carlo,³⁹ Z. Doležal,⁵ T. V. Dong,^{16,12} S. Eidelman,^{4,64,41} D. Epifanov,^{4,64} J. E. Fast,⁶⁶ T. Ferber,⁷ A. Frey,¹¹ B. G. Fulsom,⁶⁶ R. Garg,⁶⁷ V. Gaur,⁸⁹ N. Gabyshev,^{4,64} A. Garmash,^{4,64} M. Gelb,³² A. Giri,²² P. Goldenzweig,³² D. Greenwald,⁸² J. Haba,^{16,12} K. Hayasaka,⁶³ H. Hayashii,⁵⁷ W.-S. Hou,⁶⁰ C.-L. Hsu,⁷⁹ T. Iijima,^{55,54} K. Inami,⁵⁴ G. Inguglia,⁷ A. Ishikawa,⁸⁴ R. Itoh,^{16,12} M. Iwasaki,⁶⁵ Y. Iwasaki,¹⁶ W. W. Jacobs,²⁴ Y. Jin,⁸⁶ D. Joffe,³³ J. Kahn,⁴³ A. B. Kaliyar,²³ G. Karyan,⁷ T. Kawasaki,³⁵ H. Kichimi,¹⁶ C. Kiesling,⁴⁸ D. Y. Kim,⁷⁵ H. J. Kim,³⁸ J. B. Kim,³⁷ S. H. Kim,¹⁴ K. Kinoshita,⁶ P. Kodyš,⁵ S. Korpar,^{47,31} D. Kotchetkov,¹⁵ P. Križan,^{42,31} R. Kroeger,⁵⁰ P. Krokovny,^{4,64} T. Kuhr,⁴³ R. Kulasiri,³³ R. Kumar,⁷⁰ A. Kuzmin,^{4,64} Y.-J. Kwon,⁹² K. Lalwani,⁴⁵ J. S. Lange,¹⁰ I. S. Lee,¹⁴ J. Y. Lee,⁷³ S. C. Lee,³⁸ C. H. Li,⁴⁹ L. K. Li,²⁵ Y. B. Li,⁶⁸ L. Li Gioi,⁴⁸ J. Libby,²³ Z. Liptak,¹⁵ D. Liventsev,^{89,16} P.-C. Lu,⁶⁰ M. Lubej,³¹ J. MacNaughton,⁵¹ M. Masuda,⁸⁵ T. Matsuda,⁵¹ D. Matvienko,^{4,64,41} M. Merola,^{28,56} H. Miyata,⁶³ R. Mizuk,^{41,52,53} T. Mori,⁵⁴ R. Mussa,²⁹ E. Nakano,⁶⁵ M. Nakao,^{16,12} K. J. Nath,²¹ M. Nayak,^{90,16} N. K. Nisar,⁶⁹ S. Nishida,^{16,12} S. Ogawa,⁸³ S. L. Olsen,¹³ H. Ono,^{62,63} Y. Onuki,⁸⁶ W. Ostrowicz,⁶¹ G. Pakhlova,^{41,53} B. Pal,³ S. Pardi,²⁸ S. Paul,⁸² T. K. Pedlar,⁴⁴ R. Pestotnik,³¹ L. E. Piilonen,⁸⁹ V. Popov,^{41,53} E. Prencipe,¹⁸ M. Ritter,⁴³ A. Rostomyan,⁷ G. Russo,²⁸ Y. Sakai,^{16,12} M. Salehi,^{46,43} S. Sandilya,⁶ L. Santelj,¹⁶ T. Sanuki,⁸⁴ V. Savinov,⁶⁹ O. Schneider,⁴⁰ G. Schnell,^{1,19} J. Schueler,¹⁵ C. Schwanda,²⁶ Y. Seino,⁶³ K. Senyo,⁹¹ M. E. Sevier,⁴⁹ T.-A. Shibata,⁸⁷ J.-G. Shiu,⁶⁰ F. Simon,⁴⁸ A. Sokolov,²⁷ E. Solovieva,^{41,53} M. Starič,³¹ Z. S. Stottler,⁸⁹ J. F. Strube,⁶⁶ T. Sumiyoshi,⁸⁸ W. Sutcliffe,³² M. Takizawa,^{74,17,71} K. Tanida,³⁰ Y. Tao,⁸ F. Tenchini,⁷ M. Uchida,⁸⁷ S. Uehara,^{16,12} T. Uglov,^{41,53} Y. Unno,¹⁴ S. Uno,^{16,12} P. Urquijo,⁴⁹ Y. Usov,^{4,64} R. Van Tonder,³² G. Varner,¹⁵ K. E. Varvell,⁷⁹ V. Vorobyev,^{4,64,41} E. Waheed,⁴⁹ B. Wang,⁶ C. H. Wang,⁵⁹ M.-Z. Wang,⁶⁰ P. Wang,²⁵ S. Watanuki,⁸⁴ E. Widmann,⁷⁷ E. Won,³⁷ H. Yamamoto,⁸⁴ S. B. Yang,³⁷ H. Ye,⁷ J. H. Yin,²⁵ Y. Yusa,⁶³ Z. P. Zhang,⁷² V. Zhilich,^{4,64} V. Zhukova,⁴¹ and V. Zhulanov^{4,64}

(The Belle Collaboration)

¹University of the Basque Country UPV/EHU, 48080 Bilbao

²Beihang University, Beijing 100191

³Brookhaven National Laboratory, Upton, New York 11973

⁴Budker Institute of Nuclear Physics SB RAS, Novosibirsk 630090

⁵Faculty of Mathematics and Physics, Charles University, 121 16 Prague

⁶University of Cincinnati, Cincinnati, Ohio 45221

⁷Deutsches Elektronen-Synchrotron, 22607 Hamburg

⁸University of Florida, Gainesville, Florida 32611

⁹Key Laboratory of Nuclear Physics and Ion-beam Application (MOE)

and Institute of Modern Physics, Fudan University, Shanghai 200443

¹⁰Justus-Liebig-Universität Gießen, 35392 Gießen

¹¹II. Physikalisches Institut, Georg-August-Universität Göttingen, 37073 Göttingen

¹²SOKENDAI (The Graduate University for Advanced Studies), Hayama 240-0193

¹³Gyeongsang National University, Chinju 660-701

¹⁴Hanyang University, Seoul 133-791

¹⁵University of Hawaii, Honolulu, Hawaii 96822

¹⁶High Energy Accelerator Research Organization (KEK), Tsukuba 305-0801

¹⁷J-PARC Branch, KEK Theory Center, High Energy Accelerator Research Organization (KEK), Tsukuba 305-0801

¹⁸Forschungszentrum Jülich, 52425 Jülich

¹⁹IKERBASQUE, Basque Foundation for Science, 48013 Bilbao

²⁰Indian Institute of Technology Bhubaneswar, Satya Nagar 751007

²¹Indian Institute of Technology Guwahati, Assam 781039

²²Indian Institute of Technology Hyderabad, Telangana 502285

- ²³Indian Institute of Technology Madras, Chennai 600036
²⁴Indiana University, Bloomington, Indiana 47408
²⁵Institute of High Energy Physics, Chinese Academy of Sciences, Beijing 100049
²⁶Institute of High Energy Physics, Vienna 1050
²⁷Institute for High Energy Physics, Protvino 142281
²⁸INFN - Sezione di Napoli, 80126 Napoli
²⁹INFN - Sezione di Torino, 10125 Torino
³⁰Advanced Science Research Center, Japan Atomic Energy Agency, Naka 319-1195
³¹J. Stefan Institute, 1000 Ljubljana
³²Institut für Experimentelle Teilchenphysik, Karlsruher Institut für Technologie, 76131 Karlsruhe
³³Kennesaw State University, Kennesaw, Georgia 30144
³⁴Department of Physics, Faculty of Science, King Abdulaziz University, Jeddah 21589
³⁵Kitasato University, Sagami-hara 252-0373
³⁶Korea Institute of Science and Technology Information, Daejeon 305-806
³⁷Korea University, Seoul 136-713
³⁸Kyungpook National University, Daegu 702-701
³⁹LAL, Univ. Paris-Sud, CNRS/IN2P3, Université Paris-Saclay, Orsay
⁴⁰École Polytechnique Fédérale de Lausanne (EPFL), Lausanne 1015
⁴¹P.N. Lebedev Physical Institute of the Russian Academy of Sciences, Moscow 119991
⁴²Faculty of Mathematics and Physics, University of Ljubljana, 1000 Ljubljana
⁴³Ludwig Maximilians University, 80539 Munich
⁴⁴Luther College, Decorah, Iowa 52101
⁴⁵Malaviya National Institute of Technology Jaipur, Jaipur 302017
⁴⁶University of Malaya, 50603 Kuala Lumpur
⁴⁷University of Maribor, 2000 Maribor
⁴⁸Max-Planck-Institut für Physik, 80805 München
⁴⁹School of Physics, University of Melbourne, Victoria 3010
⁵⁰University of Mississippi, University, Mississippi 38677
⁵¹University of Miyazaki, Miyazaki 889-2192
⁵²Moscow Physical Engineering Institute, Moscow 115409
⁵³Moscow Institute of Physics and Technology, Moscow Region 141700
⁵⁴Graduate School of Science, Nagoya University, Nagoya 464-8602
⁵⁵Kobayashi-Maskawa Institute, Nagoya University, Nagoya 464-8602
⁵⁶Università di Napoli Federico II, 80055 Napoli
⁵⁷Nara Women's University, Nara 630-8506
⁵⁸National Central University, Chung-li 32054
⁵⁹National United University, Miao Li 36003
⁶⁰Department of Physics, National Taiwan University, Taipei 10617
⁶¹H. Niewodniczanski Institute of Nuclear Physics, Krakow 31-342
⁶²Nippon Dental University, Niigata 951-8580
⁶³Niigata University, Niigata 950-2181
⁶⁴Novosibirsk State University, Novosibirsk 630090
⁶⁵Osaka City University, Osaka 558-8585
⁶⁶Pacific Northwest National Laboratory, Richland, Washington 99352
⁶⁷Panjab University, Chandigarh 160014
⁶⁸Peking University, Beijing 100871
⁶⁹University of Pittsburgh, Pittsburgh, Pennsylvania 15260
⁷⁰Punjab Agricultural University, Ludhiana 141004
⁷¹Theoretical Research Division, Nishina Center, RIKEN, Saitama 351-0198
⁷²University of Science and Technology of China, Hefei 230026
⁷³Seoul National University, Seoul 151-742
⁷⁴Showa Pharmaceutical University, Tokyo 194-8543
⁷⁵Soongsil University, Seoul 156-743
⁷⁶University of South Carolina, Columbia, South Carolina 29208
⁷⁷Stefan Meyer Institute for Subatomic Physics, Vienna 1090
⁷⁸Sungkyunkwan University, Suwon 440-746
⁷⁹School of Physics, University of Sydney, New South Wales 2006
⁸⁰Department of Physics, Faculty of Science, University of Tabuk, Tabuk 71451
⁸¹Tata Institute of Fundamental Research, Mumbai 400005
⁸²Department of Physics, Technische Universität München, 85748 Garching
⁸³Toho University, Funabashi 274-8510
⁸⁴Department of Physics, Tohoku University, Sendai 980-8578
⁸⁵Earthquake Research Institute, University of Tokyo, Tokyo 113-0032

⁸⁶Department of Physics, University of Tokyo, Tokyo 113-0033

⁸⁷Tokyo Institute of Technology, Tokyo 152-8550

⁸⁸Tokyo Metropolitan University, Tokyo 192-0397

⁸⁹Virginia Polytechnic Institute and State University, Blacksburg, Virginia 24061

⁹⁰Wayne State University, Detroit, Michigan 48202

⁹¹Yamagata University, Yamagata 990-8560

⁹²Yonsei University, Seoul 120-749

Using data samples of 89.5 fb^{-1} , 711.0 fb^{-1} , and 121.4 fb^{-1} collected with the Belle detector at the KEKB asymmetric-energy e^+e^- collider at center-of-mass energies 10.52 GeV, 10.58 GeV, and 10.867 GeV, respectively, we study the exclusive reactions $e^+e^- \rightarrow \gamma\chi_{cJ}$ ($J = 0, 1, 2$) and $e^+e^- \rightarrow \gamma\eta_c$. A significant $\gamma\chi_{c1}$ signal is observed for the first time at $\sqrt{s} = 10.58 \text{ GeV}$ with a significance of 5.1σ including systematic uncertainties. No significant excesses for $\gamma\chi_{c0}$, $\gamma\chi_{c2}$, and $\gamma\eta_c$ final states are found, and we set 90% credibility level upper limits on the Born cross sections (σ_B) at 10.52 GeV, 10.58 GeV, and 10.867 GeV. Together with cross sections measured by BESIII at lower center-of-mass energies, the energy dependency of $\sigma_B(e^+e^- \rightarrow \gamma\chi_{c1})$ is obtained.

PACS numbers: 13.66.Bc, 13.25.Gv, 14.40.Pq

The production of heavy quark pairs in high-energy lepton collisions is described well by perturbative Quantum Chromodynamics (pQCD). Yet a description of these pairs forming quarkonium—charmonium or bottomonium—is theoretically challenging. Quarkonium formation is governed by nonperturbative long-distance effects [1]. Nonrelativistic Quantum Chromodynamics (NRQCD) factorization was used to compute the cross section for several processes, including the double-charmonium production cross section [2, 3], $e^+e^- \rightarrow \gamma\chi_{cJ}$ ($J = 0, 1, 2$) [4–8] and $e^+e^- \rightarrow \gamma\eta_c$ [5, 6, 9, 10] at B factories with relativistic and higher-order corrections included.

Electromagnetic quarkonium production is relatively simpler than other production mechanisms, and therefore it serves as a good testing ground for such NRQCD predictions. The BESIII experiment measured $e^+e^- \rightarrow \gamma\chi_{cJ}$ cross sections at $\sqrt{s} = 4.01 \text{ GeV}$, 4.23 GeV , 4.26 GeV , and 4.36 GeV and $e^+e^- \rightarrow \gamma\eta_c$ cross section at the same energies and additionally at 4.42 GeV and 4.60 GeV [11, 12]. At none of the individual energy points does the statistical significance for production of χ_{cJ} or η_c exceed 3σ , and when the data from all energy points are combined, the statistical significances for χ_{c1} , χ_{c2} , and η_c are 3.0σ , 3.4σ , and greater than 3.6σ , respectively.

In addition, the BESIII experiment reported evidence for $X(3872)$ production via $e^+e^- \rightarrow \gamma X(3872)$ [13]. Precise and unambiguous measurement of $e^+e^- \rightarrow \gamma\chi_{cJ}$ and $\gamma\eta_c$ is useful for understanding C -even quarkonia and exotic XYZ particles [14–16], e.g., $X(3872)$.

In this paper, we report cross-section measurements for the exclusive reactions $e^+e^- \rightarrow \gamma\chi_{cJ}$ and $\gamma\eta_c$ with data recorded at $\sqrt{s} \sim 10.6 \text{ GeV}$ by the Belle experiment at the KEKB asymmetric-energy e^+e^- collider [17, 18]. The data used in this analysis corresponds to 89.5 fb^{-1} of integrated luminosity at 10.52 GeV, referred to as the continuum sample; 711 fb^{-1} at 10.58 GeV, referred to as the $\Upsilon(4S)$ sample; and 121.4 fb^{-1} at 10.867 GeV, referred

to as the $\Upsilon(5S)$ sample.

The Belle detector [19, 20] is a large solid-angle magnetic spectrometer that consists of a silicon vertex detector, a 50-layer central drift chamber (CDC), an array of aerogel threshold Cherenkov counters (ACC), a barrel-like arrangement of time-of-flight scintillation counters (TOF), and an electromagnetic calorimeter comprised of CsI(Tl) crystals (ECL) located inside a superconducting solenoid coil that provides a 1.5 T magnetic field. An iron flux-return yoke instrumented with resistive plate chambers (KLM) located outside the coil is used to detect K_L^0 mesons and to identify muons. The Belle detector is described in detail elsewhere [19, 20].

We determined event-selection criteria using a large sample of Monte Carlo (MC) signal events (100k) for $e^+e^- \rightarrow \gamma\chi_{cJ}$ and $\gamma\eta_c$ at $\sqrt{s} = 10.52, 10.58$, and 10.867 GeV generated with EvtGen [21]. In the generator, the polar angle of the transition photon in the e^+e^- C.M. system (θ_γ) is distributed according to $(1 + \cos^2 \theta_\gamma)$ for $\gamma\chi_{c0}$ and $\gamma\eta_c$ production, and $(1 + 0.63 \cos^2 \theta_\gamma)$ for $\gamma\chi_{c1}$ production [22]. No definite model exists for the distribution of θ_γ in $\gamma\chi_{c2}$ production because the combination of tensor-meson production and γ emission is theoretically complicated and requires experimental input. So we model the production of this channel as evenly distributed in phase space and account for differences from $(1 \pm \cos^2 \theta_\gamma)$ distributions as systematic uncertainties.

Corrections due to initial-state radiation (ISR) are taken into account in all studied channels, where we assume $\sigma(e^+e^- \rightarrow \gamma\chi_{cJ}/\eta_c) \sim 1/s^n$ in the calculation of the radiative-correction factor. The values of n , determined from Refs. [8, 10], are 1.4 for χ_{c0} , 2.1 for χ_{c1} , 2.4 for χ_{c2} , and 1.3 for η_c in the predictions of next-to-leading order (NLO) QCD, and 1.4 for η_c in leading order (LO) QCD. Possible sources of background events from $\Upsilon(nS) \rightarrow B\bar{B}$ ($n = 4, 5$), $\Upsilon(5S) \rightarrow B_s^{(*)}\bar{B}_s^{(*)}$, and $e^+e^- \rightarrow q\bar{q}$ ($q = u, d, s, c$) are checked with a MC sample four times larger than the data sample, and are also gen-

erated with EvtGen [21]. GEANT3 [23] is used to simulate the detector response to all MC events. The χ_{cJ} candidates are reconstructed from their decays to $\gamma J/\psi$ with $J/\psi \rightarrow \mu^+\mu^-$, and the η_c candidates are reconstructed from five hadronic decays into $K_S^0 K^+\pi^-$, $\pi^+\pi^- K^+K^-$, $2(\pi^+\pi^-)$, $2(K^+K^-)$, and $3(\pi^+\pi^-)$ [24].

We define a well-reconstructed charged track as having impact parameters with respect to the nominal interaction point of less than 0.5 cm and 4 cm perpendicular to and along the beam direction, respectively. For a $e^+e^- \rightarrow \gamma\chi_{cJ}$ candidate event, we require the number of well-reconstructed charged tracks, N_{trk} , to be two, and the net charge be zero. For $e^+e^- \rightarrow \gamma\eta_c$, we require $N_{\text{trk}} = 6$ for the $3(\pi^+\pi^-)$ final state and $N_{\text{trk}} = 4$ for the other final states, also with a zero net charge. For the particle identification (PID) of a well-reconstructed charged track, information from different detector subsystems, including specific ionization in the CDC, time measurement in the TOF, and the response of the ACC, is combined to form a likelihood \mathcal{L}_i [25] for particle species i . Tracks with $R_K = \mathcal{L}_K/(\mathcal{L}_K + \mathcal{L}_\pi) < 0.4$ are identified as pions with an efficiency of 96%, while 9% of kaons are misidentified as pions; tracks with $R_K > 0.6$ are identified as kaons with an efficiency of 98%, while 8% of pions are misidentified as kaons.

For muons from $J/\psi \rightarrow \mu^+\mu^-$, we require at least one of the paired tracks to have $R_\mu = \mathcal{L}_\mu/(\mathcal{L}_\mu + \mathcal{L}_K + \mathcal{L}_\pi) > 0.95$; if one track has $R_\mu < 0.95$, it must have associated hits in the KLM agreeing with the extrapolated trajectory provided by the CDC [26]. The efficiency of muon-pair identification is 94%.

Using a multivariate analysis with a neural network [27] based on two sets of input variables [28], a K_S^0 candidate is reconstructed from a pair of oppositely-charged tracks that are treated as pions. An ECL cluster with energy higher than 50 MeV is treated as a photon candidate if it does not match the extrapolation of any charged track. The photon with the maximum energy in the e^+e^- C.M. system is taken as the transition photon. Since there are two photons in the $e^+e^- \rightarrow \gamma\chi_{cJ}$ channel, the transition photon is denoted as γ_h , and the one with the second highest energy is denoted as γ_1 and is taken as the photon from the $\chi_{cJ} \rightarrow \gamma J/\psi$ decay. We require $E(\gamma_1) > 300$ MeV to suppress the backgrounds from fake photons.

If there are more than two photons, to suppress the background from the ISR process $e^+e^- \rightarrow \gamma_{\text{ISR}}\psi(2S) \rightarrow \gamma_{\text{ISR}}\gamma\chi_{cJ}$, an extra photon (γ_{ext}) besides γ_h and γ_1 is selected, and $M(\gamma_{\text{ext}}\gamma_1\mu^+\mu^-) < 3.60$ GeV/ c^2 or $M(\gamma_{\text{ext}}\gamma_h\mu^+\mu^-) > 3.78$ GeV/ c^2 is required. This requirement removes 92.2% and 91.5% of the ISR $\psi(2S) \rightarrow \gamma\chi_{c1}$ and $\gamma\chi_{c2}$ background events, respectively. The residual yields of χ_{c1} and χ_{c2} events from ISR $\psi(2S)$ decays are expected to be 0.84 ± 0.15 and 0.43 ± 0.05 , respectively, where the uncertainties from intermediate branching fractions and $\psi(2S)$ production cross-section via ISR

are considered. The selection efficiency of this requirement is 85.5% for the χ_{c1} signal and 80.9% for the χ_{c2} one.

A four-constraint (4C) kinematic fit constraining the four-momenta of the final-state particles to the initial e^+e^- collision system is performed. In $e^+e^- \rightarrow \gamma\chi_{cJ}$, an additional constraint is used, constraining the mass of the $\mu^+\mu^-$ pair to the J/ψ nominal mass, giving a five-constraint (5C) kinematic fit. Kinematic fits with $\chi_{5C}^2 < 25$ for $e^+e^- \rightarrow \gamma\chi_{cJ}$ and $\chi_{4C}^2 < 30$ for $e^+e^- \rightarrow \gamma\eta_c$ are required to improve the resolutions of the momenta of charged tracks and the energies of photons, and to suppress backgrounds with more than two photons, such as ISR processes.

The invariant mass distribution of the $\mu^+\mu^-$ pair from the continuum, $\Upsilon(4S)$, and $\Upsilon(5S)$ data samples, prior to the application of the 5C fit, is shown in Fig. 1, together with the result of fitting the data to the sum of a Gaussian function for the J/ψ and a first order polynomial for the background. In the plot, a clear J/ψ signal is observed. We define the J/ψ signal region as $|M_{\mu^+\mu^-} - m_{J/\psi}| < 48$ MeV/ c^2 corresponding to three times the detector resolution, where $m_{J/\psi}$ is the J/ψ mass [29].

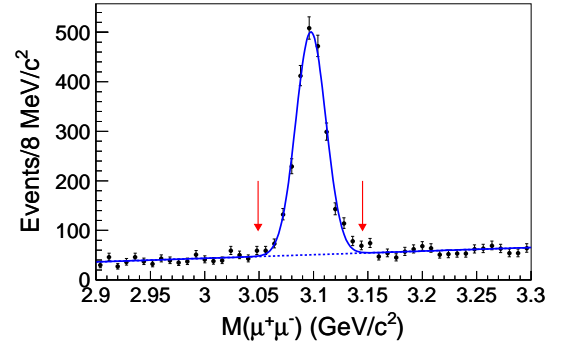


FIG. 1: The invariant mass distribution of $\mu^+\mu^-$ pairs from all the data samples before the application of the 5C kinematic fit. The solid curve is the fit, and the dotted line is the fitted background. The arrows show the boundaries of the defined J/ψ signal region.

After all of the above requirements, some non-peaking background events are observed in the processes $e^+e^- \rightarrow \gamma\chi_{cJ}$ and $\gamma\eta_c$ at the studied C.M. energy points.

Figure 2 shows the $\gamma_1 J/\psi$ invariant mass distributions for the data. A clear χ_{c1} signal is observed in the $\Upsilon(4S)$ data sample, but is not evident in the other two data samples. Unbinned extended maximum-likelihood fits to the $M_{\gamma_1 J/\psi}$ distributions are performed to extract the χ_{cJ} signal yields. The χ_{cJ} signal shapes in the fits are a Breit-Wigner (BW) function convolved with a Log-normal [30] function with all the values of the χ_{cJ} resonance parameters fixed from the fits to MC simulations; second-order polynomial functions are used to describe the background distributions. The MC-simulated χ_{cJ} signals have mass

resolutions around $6 \text{ MeV}/c^2$ with small low-mass tails due to the measurement of $E(\gamma_1)$. The results from the fits are listed in Table I. The statistical significances of the χ_{cJ} signals are calculated using $\sqrt{-2 \ln(\mathcal{L}_0/\mathcal{L}_{\max})}$, where \mathcal{L}_0 and \mathcal{L}_{\max} are the maximized likelihoods of the fits without and with the χ_{cJ} signal, respectively. The statistical significance of the χ_{c1} signal in the $\Upsilon(4S)$ sample is 5.2σ . The signal significance remains at 5.1σ when convolving the likelihood profile with a Gaussian function of width equal to the total systematic uncertainty discussed below. The χ_{cJ} signals in the continuum sample and the $\Upsilon(5S)$ sample are not significant, as indicated in Table I.

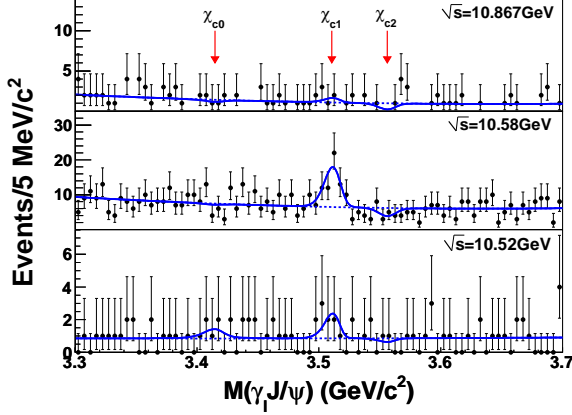


FIG. 2: The $\gamma_1 J/\psi$ invariant mass spectra at $\sqrt{s} = 10.52$ (bottom), 10.58 (middle), and 10.867 GeV (top) together with fit results. The points with error bars show the data and the solid curves are the fit functions; the dashed curves show the fitted backgrounds contributions. The arrows show the expected peak positions for the χ_{c0} , χ_{c1} , and χ_{c2} states.

Figure 3 shows the η_c invariant mass distributions for the five hadronic final states combined. Clear signals resulting from the production of J/ψ by ISR are present, while no significant η_c signal is evident.

We perform a simultaneous fit to the five η_c final states, in which the ratio of the yields in each channel is fixed to the ratio of $\mathcal{B}_i \varepsilon_i$, where i is the η_c decay-mode index, \mathcal{B}_i is the branching fraction taken from the Particle Data Group (PDG) [29], and ε_i is the reconstruction efficiency determined from MC simulation. In the fit, we use a BW function convolved with a Gaussian resolution function to describe the η_c signal; the values of all parameters are fixed from the fits to MC simulations. A Gaussian function with free parameters is used to describe the J/ψ signal, and a second-order Chebyshev polynomial function is used for the backgrounds. The fit results are shown in Fig. 3 and summarized in Table I.

The Born cross section for $e^+e^- \rightarrow \gamma X$ is given by the formula

$$\sigma_B(e^+e^- \rightarrow \gamma X) = \frac{N^{\text{obs}} \times |1 - \prod|^2}{\mathcal{L} \times \sum_i \mathcal{B}_i \varepsilon_i \times (1 + \delta)_{\text{ISR}}}, \quad (1)$$

where N^{obs} is the number of signal events obtained from the fit, \mathcal{L} is the integrated luminosity of the data sample, \mathcal{B}_i and ε_i are the branching fraction and the detection efficiency of the i -th X decay mode (χ_{cJ} is reconstructed in one decay mode and η_c in five decay modes). $(1 + \delta)_{\text{ISR}}$ is the radiative-correction factor, calculated using the formula given in Ref. [31], and $|1 - \prod|^2$ is the vacuum polarization factor, calculated according to Ref. [32]. The obtained Born cross sections for $e^+e^- \rightarrow \gamma \chi_{cJ}$ and $\gamma \eta_c$ are listed in Table I together with all the parameter results needed for the cross section calculation.

For all processes but $e^+e^- \rightarrow \gamma \chi_{c1}$ at $\sqrt{s} = 10.58 \text{ GeV}$, upper limits at 90% credibility level (C.L.) [33] on the numbers of signal events (N^{UL}) and the Born cross sections (σ_B^{UL}) are determined by solving the equation

$$\frac{\int_0^{x^{\text{UL}}} \mathcal{F}_{\text{likelihood}}(x) dx}{\int_0^{+\infty} \mathcal{F}_{\text{likelihood}}(x) dx} = 90\%, \quad (2)$$

where x is the assumed signal yield or Born cross section, and $\mathcal{F}_{\text{likelihood}}(x)$ is the corresponding maximized likelihood from a fit to the data. To take into account the systematic uncertainties discussed below, the likelihood is convolved with a Gaussian function whose width equals the corresponding systematic uncertainty.

Combining the measurement of $\sigma_B(e^+e^- \rightarrow \gamma \chi_{c1})$ from BESIII [11] and this analysis, we show the cross section as a function of \sqrt{s} in Fig. 4. We fit these data points with a function proportional to $1/s^n$ assuming that the reaction $e^+e^- \rightarrow \gamma \chi_{c1}$ proceeds through the continuum process only: from a fit to the seven points for $e^+e^- \rightarrow \gamma \chi_{c1}$, we find $n = 2.1^{+0.3}_{-0.4}$. The significance of the fitted n is 2.2σ , calculated using $\sqrt{\chi_0^2 - \chi_{\min}^2} = 2.2$, where χ_0^2 is the χ^2 with n fixed at 0, and χ_{\min}^2 is the mini-

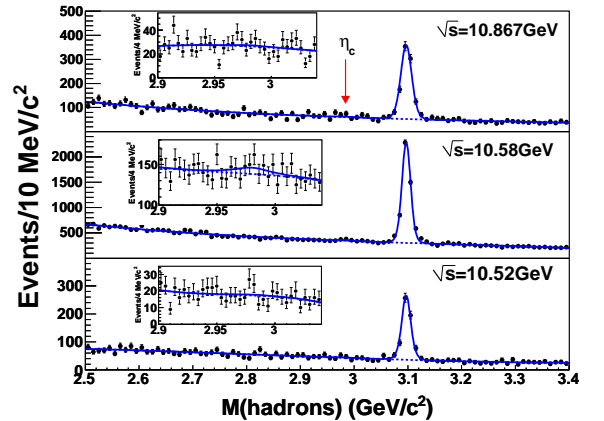


FIG. 3: The mass distributions for the sum of the five η_c decay modes at $\sqrt{s} = 10.52$ (bottom), 10.58 (middle), and 10.867 GeV (top). The points with error bars show the data and the curves show the best-fit results; the dashed curves show the backgrounds contributions. The insets show the η_c region. The J/ψ signals are produced via ISR.

TABLE I: Measurements of $e^+e^- \rightarrow \gamma\chi_{cJ}$ and $e^+e^- \rightarrow \gamma\eta_c$ at $\sqrt{s} = 10.52$ GeV, 10.58 GeV, and 10.867 GeV. $\varepsilon(\%)$ represents efficiency for the $e^+e^- \rightarrow \gamma\chi_{cJ}$, and value of $\Sigma_i \mathcal{B}_i \varepsilon_i$ for the $e^+e^- \rightarrow \gamma\eta_c$. $\Sigma(\sigma)$ is the statistical signal significance; $\sigma_{\text{syst}}(\%)$ is the systematic uncertainty on σ_B . The Born cross sections are given with statistical (first) and systematic (second) uncertainties.

| Channel | \sqrt{s} (GeV) | N^{obs} | N^{UL} | $\Sigma(\sigma)$ | $\varepsilon(\%)$ | $ 1 - \prod ^2$ | $(1 + \delta)_{\text{ISR}}$ | $\sigma_{\text{syst}}(\%)$ | σ_B (fb) | σ_B^{UL} (fb) |
|--------------------------------------|------------------|------------------------|-----------------|------------------|-------------------|-----------------|-----------------------------|----------------------------|------------------------------------|-----------------------------|
| $e^+e^- \rightarrow \gamma\chi_{c0}$ | 10.52 | $2.9^{+4.0}_{-3.3}$ | 9.6 | 0.9 | 19.0 | 0.931 | 0.732868 | 10.7 | $286.2^{+394.7}_{-325.6} \pm 30.7$ | 957.2 |
| $e^+e^- \rightarrow \gamma\chi_{c1}$ | | $4.8^{+3.6}_{-2.9}$ | 10.4 | 1.9 | 20.8 | | 0.733432 | 8.9 | $16.2^{+12.1}_{-9.8} \pm 1.4$ | 34.9 |
| $e^+e^- \rightarrow \gamma\chi_{c2}$ | | $-0.8^{+2.3}_{-1.6}$ | 4.5 | - | 19.9 | | 0.733675 | 12.8 | $-5.0^{+14.3}_{-10.0} \pm 0.6$ | 28.9 |
| $e^+e^- \rightarrow \gamma\eta_c$ | | $6.8^{+14.8}_{-14.3}$ | 30.8 | 0.5 | 0.79 | | 0.732788 | 11.3 | $9.0^{+19.5}_{-18.8} \pm 1.0$ | 40.6 |
| $e^+e^- \rightarrow \gamma\chi_{c0}$ | 10.58 | $-1.6^{+9.8}_{-8.9}$ | 16.5 | - | 18.9 | 0.930 | 0.732725 | 13.1 | $-20.0^{+122.3}_{-111.0} \pm 2.6$ | 205.9 |
| $e^+e^- \rightarrow \gamma\chi_{c1}$ | | $39.0^{+9.5}_{-8.8}$ | - | 5.2 | 19.9 | | 0.73329 | 10.0 | $17.3^{+4.2}_{-3.9} \pm 1.7$ | - |
| $e^+e^- \rightarrow \gamma\chi_{c2}$ | | $-8.7^{+5.7}_{-5.0}$ | 7.2 | - | 19.8 | | 0.733532 | 20.9 | $-6.8^{+4.5}_{-3.9} \pm 1.4$ | 5.7 |
| $e^+e^- \rightarrow \gamma\eta_c$ | | $67.2^{+42.0}_{-39.2}$ | 125.9 | 1.8 | 0.78 | | 0.732645 | 13.0 | $11.3^{+7.0}_{-6.6} \pm 1.5$ | 21.1 |
| $e^+e^- \rightarrow \gamma\chi_{c0}$ | 10.867 | $-1.3^{+4.0}_{-3.2}$ | 7.0 | - | 17.7 | 0.929 | 0.732054 | 9.4 | $-101.4^{+312.0}_{-249.6} \pm 9.5$ | 543.7 |
| $e^+e^- \rightarrow \gamma\chi_{c1}$ | | $1.9^{+3.4}_{-2.6}$ | 7.9 | 0.7 | 16.8 | | 0.73262 | 13.4 | $5.8^{+10.5}_{-8.0} \pm 0.8$ | 24.3 |
| $e^+e^- \rightarrow \gamma\chi_{c2}$ | | $-2.8^{+3.2}_{-2.4}$ | 5.3 | - | 16.3 | | 0.732863 | 14.4 | $-15.7^{+17.9}_{-13.4} \pm 2.3$ | 30.3 |
| $e^+e^- \rightarrow \gamma\eta_c$ | | $12.3^{+18.2}_{-17.4}$ | 42.3 | 0.9 | 0.76 | | 0.731974 | 9.1 | $12.3^{+17.3}_{-18.1} \pm 1.1$ | 42.2 |

mum χ^2 with the value of n free, respectively. Adding an additional possible resonance, such as $\psi(4040)$, $\psi(4160)$, $Y(4260)$, or $\Upsilon(4S)$, the largest change in the fitted value of n is 0.3. The result is consistent with the prediction by NRQCD with all leading relativistic corrections included in Ref. [8]. Due to the large uncertainties, we do not fit the \sqrt{s} dependence of $e^+e^- \rightarrow \gamma\chi_{c0}$, $e^+e^- \rightarrow \gamma\chi_{c2}$, or $e^+e^- \rightarrow \gamma\eta_c$.

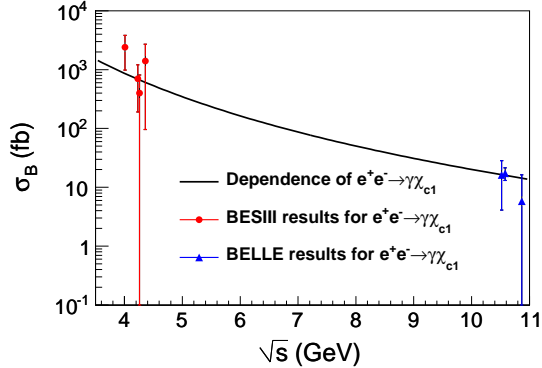


FIG. 4: Measured cross sections for $e^+e^- \rightarrow \gamma\chi_{c1}$ as a function of C.M. energy. Error bars contain both the statistical and systematic uncertainties. The curve shows the result of fit with a function proportional to $1/s^n$.

There are several sources of systematic uncertainty in the Born cross section measurements, including detection efficiency, the statistical error of the MC efficiency, trigger simulation, intermediate state branching fractions, resonance parameters, the distribution of θ_γ

for $e^+e^- \rightarrow \gamma\chi_{c2}$, fit uncertainty, the s dependence of the cross sections, and the integrated luminosity. The systematic uncertainty for detection efficiency is a final-state-dependent combined uncertainty for all the different types of particles detected, including tracking efficiency, PID, K_S^0 selection, and photon reconstruction.

Based on a study of $D^{*+} \rightarrow D^0(\rightarrow K_S^0 \pi^+ \pi^-) \pi^+$, the uncertainty in tracking efficiency is taken to be 0.35% per track. The uncertainties in PID are studied via $\gamma\gamma \rightarrow \ell^+ \ell^-$ for leptons and a low-background sample of D^* decay for charged kaons and pions. The studies show uncertainties of 2.2% for each muon, 1.0% for each charged kaon, and 1.2% for each charged pion.

Comparison of the K_S^0 selection efficiencies determined from data and MC results in $1 - \frac{\varepsilon_{\text{data}}}{\varepsilon_{\text{MC}}} = (1.4 \pm 0.3)\%$; 1.7% is taken as a conservative systematic uncertainty. The uncertainty in the photon reconstruction is 2.0% per photon, according to a study of radiative Bhabha events. For each final state, the final detection efficiency uncertainty is obtained by adding all sources in quadrature.

The statistical uncertainty in the determination of efficiency from MC is less than 1.0%. We include uncertainties of 4.8% and 0.6% from trigger simulations for $e^+e^- \rightarrow \gamma\chi_{cJ}$ and $\gamma\eta_c$, respectively. The uncertainties from the intermediate decay branching fractions are taken from Ref. [29]. For $e^+e^- \rightarrow \gamma\chi_{cJ}$, the total uncertainties from the branching fractions are obtained by adding all relative uncertainties in quadrature. For $e^+e^- \rightarrow \gamma\eta_c$, the total uncertainty from the branching fraction is obtained by summing in quadrature over the five decay modes with weight factors equal to the corresponding efficiency. The uncertainties from the resonance

parameters are estimated by changing the values of mass and width of a resonance by 1σ in the fits [29]. Additionally, for the mode $e^+e^- \rightarrow \gamma\chi_{c2}$, the uncertainty from simulating the θ_γ dependence is estimated to be 8.2% by comparing the difference between a phase space distribution and the angular distributions of $(1 \pm \cos^2\theta_\gamma)$.

In determining the number of signal events from the fits to data, the fit range and the choice of the function to describe the backgrounds are the main sources of systematic uncertainty. For the latter, the background shapes are replaced by an exponential form or a higher-order Chebyshev polynomial, and the largest difference compared to the nominal fit result is taken as the related systematic uncertainty. Changing the s dependence of the cross sections from fitted values of n to a large number, e.g., $n = 4$, gives very small differences in the radiative-correction factor ($< 1\%$). The total luminosity is determined to 1.4% precision using wide-angle Bhabha scattering events. All the uncertainties are summarized in Table II and, assuming all the sources are independent, summed in quadrature for the total systematic uncertainties.

In summary, we perform measurements of $e^+e^- \rightarrow \gamma\chi_{cJ}$ ($J = 0, 1, 2$) and $\gamma\eta_c$ at $\sqrt{s} = 10.52$ GeV, 10.58 GeV, and 10.867 GeV using a 921.9 fb $^{-1}$ data sample taken by the Belle detector. A clear χ_{c1} signal is observed at 10.58 GeV with a statistical significance of 5.2σ , and the Born cross section is measured to be $(17.3^{+4.2}_{-3.9}(\text{stat.}) \pm 1.7(\text{syst.}))$ fb. For the cases where a χ_{cJ} or η_c signal is not evident, upper limits on the Born cross sections are determined at 90% C.L. Using the cross sections measured at three different \sqrt{s} in this analysis and from BESIII at much lower \sqrt{s} and assuming the reaction $e^+e^- \rightarrow \gamma\chi_{c1}$ proceeds through the continuum process only, we determine the cross section s -dependence to be $1/s^{2.1 \pm 0.3 \pm 0.3}$ for $e^+e^- \rightarrow \gamma\chi_{c1}$.

We thank the KEKB group for the excellent operation of the accelerator; the KEK cryogenics group for the efficient operation of the solenoid; and the KEK computer group, the National Institute of Informatics, and the Pacific Northwest National Laboratory (PNNL) Environmental Molecular Sciences Laboratory (EMSL) computing group for valuable computing and Science Information NETwork 5 (SINET5) network support. We acknowledge support from the Ministry of Education, Culture, Sports, Science, and Technology (MEXT) of Japan, the Japan Society for the Promotion of Science (JSPS), and the Tau-Lepton Physics Research Center of Nagoya University; the Australian Research Council; Austrian Science Fund under Grant No. P 26794-N20; the National Natural Science Foundation of China under Contracts No. 11435013, No. 11475187, No. 11521505, No. 11575017, No. 11675166, No. 11705209; Key Research Program of Frontier Sciences, Chinese Academy of Sciences (CAS), Grant No. QYZDJ-SSW-SLH011; the CAS Center for Excellence in Particle Physics

(CCEPP); the Ministry of Education, Youth and Sports of the Czech Republic under Contract No. LTT17020; the Carl Zeiss Foundation, the Deutsche Forschungsgemeinschaft, the Excellence Cluster Universe, and the VolkswagenStiftung; the Department of Science and Technology of India; the Istituto Nazionale di Fisica Nucleare of Italy; National Research Foundation (NRF) of Korea Grants No. 2014R1A2A2A01005286, No. 2015R1A2A2A01003280, No. 2015H1A2A1033649, No. 2016R1D1A1B01010135, No. 2016K1A3A7A09005 603, No. 2016R1D1A1B02012900; Radiation Science Research Institute, Foreign Large-size Research Facility Application Supporting project and the Global Science Experimental Data Hub Center of the Korea Institute of Science and Technology Information; the Polish Ministry of Science and Higher Education and the National Science Center; the Ministry of Science and Higher Education and Russian Science Foundation (MSHE and RSF), Grant No. 18-12-00226 (Russia); the Slovenian Research Agency; Ikerbasque, Basque Foundation for Science, Basque Government (No. IT956-16) and Ministry of Economy and Competitiveness (MINECO) (Juan de la Cierva), Spain; the Swiss National Science Foundation; the Ministry of Education and the Ministry of Science and Technology of Taiwan; and the United States Department of Energy and the National Science Foundation.

-
- [1] N. Brambilla *et al.*, Eur. Phys. J. C **74**, 2981 (2014).
 - [2] Y. J. Zhang, Y. J. Gao and K. T. Chao, Phys. Rev. Lett. **96**, 092001 (2006).
 - [3] Y. J. Zhang and K. T. Chao, Phys. Rev. Lett. **98**, 092003 (2007).
 - [4] H. S. Chung, J. Lee and C. Yu, Phys. Rev. D **78**, 074022 (2008).
 - [5] W. L. Sang and Y. Q. Chen, Phys. Rev. D **81**, 034028 (2010).
 - [6] D. Li, Z. G. He and K. T. Chao, Phys. Rev. D **80**, 114014 (2009).
 - [7] G. Z. Xu, Y. J. Li, K. Y. Liu and Y. J. Zhang, JHEP **1410**, 71 (2014).
 - [8] N. Brambilla, W. Chen, Y. Jia, V. Shtabovenko and A. Vairo, Phys. Rev. D **97**, 096001 (2018).
 - [9] M. A. Shifman and M. I. Vysotsky, Nucl. Phys. B **186**, 475 (1981).
 - [10] L. B. Chen, Y. Liang and C. F. Qiao, JHEP **1801**, 091 (2018).
 - [11] M. Ablikim *et al.* (BESIII Collaboration), Chin. Phys. C **39**, 041001 (2015).
 - [12] M. Ablikim *et al.* (BESIII Collaboration), Phys. Rev. D **96**, 051101(R) (2017).
 - [13] M. Ablikim *et al.* (BESIII Collaboration), Phys. Rev. Lett. **112**, 092001 (2014).

TABLE II: Relative systematic uncertainties (%) in the cross-section measurements for $e^+e^- \rightarrow \gamma\chi_{cJ}$ and $\gamma\eta_c$ at $\sqrt{s} = 10.52$ GeV, 10.58 GeV, and 10.867 GeV. When three values are given in a cell, they apply to χ_{c0} , χ_{c1} , and χ_{c2} , respectively; otherwise a single number applies to all states.

| Final state | $\gamma\chi_{c0}/\chi_{c1}/\chi_{c2}$ | | | $\gamma\eta_c$ | | |
|------------------------------|---------------------------------------|----------------|---------------|----------------|-------|--------|
| C.M. energy (GeV) | 10.52 | 10.58 | 10.867 | 10.52 | 10.58 | 10.867 |
| Detection efficiency | 6.0 | 6.0 | 6.0 | 2.8 | 2.9 | 3.0 |
| MC sample size | 1.0 | 1.0 | 1.0 | 1.0 | 1.0 | 1.0 |
| Trigger | 4.8 | 4.8 | 4.8 | 0.6 | 0.6 | 0.6 |
| Branching fractions | 4.8/3.7/3.8 | 4.8/3.7/3.8 | 4.8/3.7/3.8 | 7.5 | 7.6 | 7.7 |
| Resonance parameters | 1.7/0.3/0.7 | 2.0/0.2/0.1 | 0.9/0.4/2.1 | 0.6 | 1.7 | 2.0 |
| θ_γ distribution | -/-/8.2 | -/-/8.2 | -/-/8.2 | - | - | - |
| Fit uncertainty | 5.3/1.9/4.5 | 9.1/5.0/17.1 | 1.4/10.3/7.7 | 7.7 | 9.8 | 2.6 |
| Integrated luminosity | 1.4 | 1.4 | 1.4 | 1.4 | 1.4 | 1.4 |
| Sum in quadrature | 10.7/8.9/12.8 | 13.1/10.0/20.9 | 9.4/13.4/14.4 | 11.3 | 13.0 | 9.1 |

- [14] L. Ma, Z. F. Sun, X. H. Liu, W. Z. Deng, X. Liu and S. L. Zhu, Phys. Rev. D **90**, 034020 (2014).
- [15] K. T. Chao, Z. G. He, D. Li and C. Meng, arXiv:1310.8597.
- [16] J. J. Dudek, R. Edwards and C. E. Thomas, Phys. Rev. D **79**, 094504 (2009).
- [17] S. Kurokawa and E. Kikutani, Nucl. Instr. and Methods Phys. Res. Sect. A **499**, 1 (2003), and other papers included in this volume.
- [18] T. Abe *et al.*, Prog. Theor. Exp. Phys. **2013**, 03A001 (2013) and references therein.
- [19] A. Abashian *et al.* (Belle Collaboration), Nucl. Instr. and Methods Phys. Res. Sect. A **479**, 117 (2002).
- [20] J. Brodzicka *et al.*, Prog. Theor. Exp. Phys. **2012**, 04D001 (2012).
- [21] D. J. Lange, Nucl. Instr. and Methods Phys. Res. Sect. A **462**, 152 (2001).
- [22] Y. Tosa, Report No. DPNU-34-1976, <http://inspirehep.net/record/109354>.
- [23] R. Brun *et al.*, GEANT 3.21, CERN Report DD/EE/84-1 (1984).
- [24] Charge-conjugate decays are implicitly assumed throughout the paper.
- [25] E. Nakano, Nucl. Instr. and Methods Phys. Res. Sect. A **494**, 402 (2002).
- [26] A. Abashian *et al.*, Nucl. Instr. and Methods Phys. Res. Sect. A **491**, 69 (2002).
- [27] M. Feindt and U. Kerzel, Nucl. Instr. and Methods Phys. Res. Sect. A **559**, 190 (2006).
- [28] H. Nakano, Ph.D. Thesis, Tohoku University (2014). Chapter 4, unpublished.
- [29] M. Tanabashi *et al.* (Particle Data Group), Phys. Rev. D **98**, 030001 (2018).
- [30] The Log-normal function is defined as $f(x) = N_0 \times \exp[-\frac{1}{2}(\ln^2(1 + \Lambda(x - x_0))/\tau^2 + \tau^2)]$ with $\Lambda = \sinh(\tau\sqrt{\ln 4})/(\sigma\sqrt{\ln 4})$. The parameters represent the mean (x_0), the width (σ), and the tail asymmetry (τ).
- [31] E. A. Kuraev and V. S. Fadin, Yad. Fiz. **41**, 733 (1985) [Sov. J. Nucl. Phys. **41**, 466 (1985)].
- [32] S. Actis *et al.*, Eur. Phys. J. C **66**, 585 (2010).
- [33] In common high-energy physics usage, this Bayesian interval has been reported as the “confidence interval,” which is a frequentist-statistics term.